Physicochemical Characterization of an Antagonistic Human Interleukin-6 Dimer[†]

Jacqueline M. Matthews,[‡] Annet Hammacher,[‡] Geoffrey J. Howlett,[§] and Richard J. Simpson*[,‡]

Joint Protein Structure Laboratory, Ludwig Institute for Cancer Research (Melbourne) and Walter and Eliza Hall Institute of Medical Research, P.O. 2008, Royal Melbourne Hospital, Parkville, 3050, Victoria, Australia, and Department of Biochemistry and Molecular Biology, University of Melbourne, Parkville, 3052, Australia

Received January 16, 1998; Revised Manuscript Received April 20, 1998

ABSTRACT: A noncovalently bound dimeric form of recombinant human IL-6 interleukin-6 (IL-6_D) was shown to be an antagonist for IL-6 activity, in a STAT3 tyrosine phosphorylation assay using HepG2 cells, under conditions where it does not dissociate into monomeric IL-6 (IL-6_M). The fluorescence from Trp157, the single tryptophan residue in the primary sequence of IL-6, is altered in IL-6_D, where the wavelength maximum is blue-shifted by 3 nm and the emission intensity is reduced by 30%. These data suggest that Trp157 is close to, but not buried by, the dimer interface. Both IL-6_D and IL-6_M are compact molecules, as determined by sedimentation velocity analysis, and contain essentially identical levels of secondary and tertiary structure, as determined by far- and near-UV CD, respectively. IL-6_D and IL-6_M show the same susceptibility to limited proteolytic attack, and exhibit identical far-UV CD-monitored urea-denaturation profiles with the midpoint of denaturation occurring at 6.0 ± 0.1 M urea. However, IL-6_D was found to dissociate prior to the complete unfolding of the protein, with a midpoint of dissociation of 3 M urea, suggesting that dissociation and dimerization occur when the protein is in a partially unfolded state. Based on these results, we suggest that IL-6_D is a metastable domain-swapped dimer, comprising two monomeric units where identical helices from each protein chain are swapped through the loop regions at the "top" of the protein (i.e., the region of the protein most distal from the N- and C-termini). Such an arrangement would account for the antagonistic activity of IL-6_D. In this model, receptor binding *site I*, which comprises residues in the A/B loop and the C-terminus of the protein, is free to bind the IL-6 receptor. However, *site III*, which includes Trp157 and residues in the C/D loop and N-terminal end of helix D, and perhaps *site II*, which comprises residues in the A and C helices, are no longer able to bind the signal transducing component of the IL-6 receptor complex, gp130.

Interleukin-6 (IL-6)[1] is a pleiotropic cytokine that plays a central role in tissue injury and host defense mechanisms to infection (*1*−*3*). The dysregulated production of IL-6 is associated with rheumatoid arthritis, psoriasis, and postmenopausal osteoporosis (*4*). While IL-6 also plays a major role in the advancement of multiple myeloma (*5*), it has been shown recently that a virally encoded homologue of IL-6 (*6*) is an apparent means by which Kaposi's sarcoma-associated herpesvirus (KSHV) can trigger the onset of multiple myeloma (*7*). This viral IL-6 may play similar roles in other diseases which are associated with KSHV including Kaposi's sarcoma and multicentric Castleman's disease. It is anticipated that treatment of these diseases may be achieved through the selective inhibition of IL-6 activity, through protein or peptide antagonists of IL-6.

IL-6 belongs to a family of four-α-helical bundle cytokines and growth factors with the up-up-down-down topology originally predicted by Bazan (*8*), and confirmed by structural studies (*9*−*12*). Many chimeric and mutagenic studies have defined three receptor binding sites, where *site I* binds the specific IL-6 receptor (IL-6R), and *sites II* and *III* bind to a second cell surface receptor, gp130 (reviewed in ref *3*).

IL-6 binds with low affinity to IL-6R to form a binary complex which then associates with high affinity to gp130 (*13*), resulting in intracellular signaling. Anything that prevents the formation of these binary or ternary receptor complexes is a potential antagonist for IL-6 activity. Both crystal and solution structures of IL-6 have recently been published (*10, 12*) as has the crystal structure of a cytokine binding region of gp130 (*14*), but, as yet, there have been no published reports of structures for IL-6R, or the higher complexes of these molecules.

The ternary complex of the IL-6 receptor system contains two molecules each of IL-6, IL-6R, and gp130 (*15*, *16*), although a model of a 1:1:2 complex, containing one molecule each of IL-6 and IL-6R and two molecules of

[†] This work was supported by Grant 950824 from the National Health and Medical Research Council of Australia.

* To whom correspondence should be addressed at the Ludwig Institute for Cancer Research, P.O. Box 2008, Royal Melbourne Hospital, Parkville, Victoria, 3050, Australia. Telephone: +61-3-9341-3155. Fax: +61-3-9341-3192. Email: Richard.Simpson@ludwig.edu.au.

[‡] Ludwig Institute for Cancer Research and Walter and Eliza Hall Institute of Medical Research.

[§] University of Melbourne.

[1] Abbreviations: CD, circular dichroism; h, human; m, murine; IL-6, interleukin-6; IL-6_D, dimeric hIL-6; IL-6_M, monomeric hIL-6; IL-6R, IL-6 receptor α-chain; gp130, IL-6 receptor β-chain; CNTF, ciliary neurotrophic factor; IL-5, interleukin-5; IL-10, interleukin-10; INF, interferon; PBS, phosphate-buffered saline (20 mM phosphate, 150 mM NaCl, pH 7.4); RP-HPLC, reversed-phase high-performance liquid chromatography; SEC, size-exclusion chromatography; STAT3, *S*ignal *T*ransducer and *A*ctivator of *T*ranscription 3; TFA, trifluoroacetic acid.

S0006-2960(98)00127-5 CCC: $15.00
Published on Web 07/10/1998

gp130, has also been proposed (*17*). There have been many observations of IL-6 dimers in preparations from natural and recombinant sources (*18, 19*) as well as in cross-linking studies of the cell surface ternary complex (*20*). Although these dimers have not been well characterized, it has been proposed that IL-6 dimerization plays a role in the formation of the ternary complex (*18, 21, 22*), and several current models of the 2:2:2 ternary complex suggest the contact of the two IL-6 molecules (*16, 23*).

We have shown recently that a noncovalently linked, dimeric form of *Escherichia coli*-derived human IL-6 (IL-6_D) interacts with the extracellular portion of IL-6R (sIL-6R) in a 1:2 complex, compared with the 1:1 complex formed by monomeric IL-6 (IL-6_M) and sIL-6R (*15*) both in solution, as detected by size-exclusion chromatography and sedimentation equilibrium analysis, and with immobilized IL-6R, as detected by surface plasmon resonance techniques (*24*). However, the IL-6_D/sIL-6R complex does not interact further with soluble recombinant gp130 (*24*). The residual bioactivity associated with IL-6_D appears to stem from the dissociation of inactive IL-6_D into active IL-6_M at 37 °C, rather than from IL-6_D itself (*24*). Further, a model of the IL-6 ternary complex from this laboratory, in which steric considerations and the Ig-like domains of gp130 play an important role, suggests that the two IL-6 molecules do not make any contact (*3*). This ability to bind to IL-6R without activating gp130 suggests that a stable, covalently linked form of IL-6_D would form a potential antagonist for IL-6 activity.

In this paper, we show that IL-6_D is an antagonist under conditions where it does not dissociate into IL-6_M. We have undertaken a full characterization of IL-6_D and find that it is a metastable dimer which dissociates when the protein is partially unfolded. Moreover, we show that the dimer is a long rodlike structure composed of two monomer-like four-α-helical bundles which make contact through the region close to Trp157 at the ends of each bundle distal from the N- and C-termini of the protein. From these studies, we propose that the dimer may be stabilized by the interchange of identical helices (the D or the C, D, and E helices) between bundles via the loop regions near Trp157.

MATERIALS AND METHODS

Production of Recombinant IL-6. Recombinant human IL-6 was produced in *Escherichia coli* and purified as described previously (*15*). Protein concentrations were estimated by the absorbance at 280 nm using an extinction coefficient of 0.47 cm^{-1} mg^{-1} mL.

Isolation of IL-6_D and IL-6_M. Lyophilized IL-6 was dissolved in water at protein concentrations >1 mg/mL, and IL-6_M and IL-6_D were isolated using size-exclusion chromatography (SEC) on a 300 × 10 mm Superose12 column (Pharmacia, Uppsala, Sweden) using a Perkin-Elmer series 4 liquid chromatograph at room temperature. Proteins were eluted with 150 mM NaCl buffered with 20 mM phosphate at pH 7.4 (PBS) and detected by the absorbance at 215 or 280 nm. Relative quantities of IL-6_M and IL-6_D were estimated by measurement of peak heights.

STAT3 Phosphorylation Assay. Following isolation of IL-6_M and IL-6_D by SEC, to prevent temperature-induced dissociation of IL-6_D into IL-6_M, the proteins were kept on ice until they were used in a *S*ignal *T*ransducer and *A*ctivator of *T*ranscription *3* (STAT3; *25*) phosphorylation assay (*24*). Induction of tyrosine phosphorylation of STAT3 in human hepatoma HepG2 cells was performed as described previously (*24*), except that the cells were stimulated with IL-6 for 50 min on ice. Samples were immunoprecipitated using phosphotyrosine antibodies (UBI, Lake Placid, NY), analyzed under reducing conditions on precast 4−20% SDS gels (Novex, San Diego, CA) using SeeBlue prestained standards, and transferred to polyvinyl difluoride membrane (Bio-Rad). Tyrosine-phosphorylated STAT3 was visualized using anti-STAT3 antibodies (Transduction Laboratories) followed by peroxidase-conjugated goat anti-mouse immunoglobulin and enhanced chemiluminescence. Densitometric scanning was performed on a model 300 Series Computing Densitometer (Molecular Dynamics, Sunnyvale, CA).

Analytical Ultracentrifugation. Sedimentation experiments were conducted using a Beckman XL-A analytical ultracentrifuge equipped with absorption optics, using an An60-Ti rotor with cells containing quartz windows and double-sector charcoal-filled Epon centerpieces. Equilibrium distributions, acquired at 0.001 cm radial increments and averaged over five measurements, were fitted for molecular weight by standard numerical analysis using the program SEDEQ1B (kindly provided by Dr. A. Minton, NIH, Bethesda). The partial specific volume of IL-6 (0.73 cm^3/g) and solution densities were calculated using the program SEDNTERP (*26*). Sedimentation coefficients were calculated from absorbance scans taken during the approach to sedimentation equilibrium, and analyzed using the program SEDFIT (*27*).

Prediction of Sedimentation Coefficients. Theoretical sedimentation coefficients for IL-6 monomer and dimer were calculated as follows. Simple computer modeling (InsightII; Biosym Technologies, San Diego, CA) was employed to construct two dimer models using the coordinates of a homology model of monomeric mouse IL-6 (*28*) which was based on the crystal structure of human granulocyte colony-stimulating factor (G-CSF; *29*). The two dimer models represent two extremes—a long "end-to-end" dimer, and a more compact "side-to-side" dimer (no molecular dynamics or energy minimization steps were taken). The monomeric and two dimeric structures were used to generate corresponding bead models (*30*) where equal sized beads were placed at the coordinates of the α-carbons so that the weight and density of the resulting model equaled those calculated from the amino acid composition. These models were used to calculate theoretical values for sedimentation and translational diffusion coefficients using the program HYDRO and the method described by Garcia de la Torres et al. (*31*). Values used for the molar mass and hydration of IL-6 were calculated as described by Laue et al. (*26*).

Spectroscopic Measurements. All spectral measurements were made in the presence of PBS. Fluorescence data were collected on a Perkin-Elmer LS5 luminescence spectrophotometer using 0.5 cm path length cells at 25 °C and 5 nm slit widths. The excitation wavelength was 295 nm, and the emission was monitored from 320 to 360 nm. Circular dichroism measurements were performed at 25 °C using an Aviv Model 62DS (Lakewood, NJ) CD spectrometer. All spectra are reported in terms of mean residue ellipticity, $[\Theta]_{MRW}$. Far-UV CD spectra were recorded using a 0.1 cm pathlength cell with protein concentrations of 0.1 mg/mL,

using an averaging time of 2 s, a bandwidth of 1 nm, and a step size of 1 nm. Reported spectra are the average of three scans with baseline subtractions. Estimates of secondary structural content were made using the reference spectra of Yang et al. (*32*) and a multilinear regression program (Prosec) supplied by Aviv. Near-UV spectra were recorded using a 1 cm path length cell with protein concentrations of 0.5 mg/mL, using an averaging time of 10 s, bandwidth of 0.5 nm, and step size of 0.2 nm. Reported spectra are baseline subtracted.

Urea-Induced Unfolding. Urea-induced unfolding of IL-6_M and IL-6_D was monitored by the changes in the CD signal at 222 nm as a function of urea concentration using protein concentrations of 0.05−0.1 mg/mL. These same samples were analyzed for IL-6_M/IL-6_D content by SEC as described above, after 16 h or 28 days at 4 °C. Relative quantities of IL-6_M and IL-6_D were estimated using maximum peak heights, and the percentages of IL-6_D remaining are reported, assuming that the percentage of IL-6_D in the absence of urea was 100%.

Dissociation of IL-6_D at 37 °C or in Urea at 25 °C. The dissociation of IL-6_D into IL-6_M in PBS at 37 °C was monitored by SEC. Stock solutions of IL-6_D at protein concentrations of 0.048 and 0.48 mg/mL were placed at 4 or 37 °C, and aliquots for each time point were analyzed immediately, or were kept at 4 °C until analysis could take place. Relative quantities of IL-6_M and IL-6_D were estimated using maximum peak heights, and the percentages of IL-6_D remaining are reported. The urea-induced dissociation of IL-6_D in PBS at 25 °C was also assessed by diluting IL-6_D into PBS or PBS containing 3 or 5 M urea (final concentrations). At selected time points, an aliquot of these urea stocks was diluted 10-fold with cold PBS and kept at 4 °C until measurements of IL-6_M and IL-6_D could be made using SEC. To examine whether the removal of IL-6 from urea during the SEC analysis had any effect on the dissociation process, we ran the SEC column in PBS, pH 7.4, containing 3 M urea. Samples which had been pre-equilibrated in 3 or 5 M urea showed identical IL-6_M:IL-6_D ratios when the elution buffer contained no urea or 3 M urea. Samples which had been equilibrated in the absence of urea showed a decrease in the relative amounts of dimer only when the elution buffer contained 3 M urea.

Limited Proteolytic Digestion. Samples were incubated with thermolysin (Boehringer Mannheim, Mannheim, Germany) using a 1:20 mass ratio of enzyme to substrate, using a sample buffer of PBS or 20 mM Tris-HCl, 150 mM NaCl, pH 7.4, at 25 °C in the presence or absence of urea. Samples for each time point were analyzed by reversed-phase high-performance liquid chromatography (RP-HPLC) on an Hewlett-Packard 1090A liquid chromatograph utilizing a TFA/acetonitrile gradient.

RESULTS

IL-6_D Is an IL-6 Antagonist under Conditions Where It Does Not Dissociate. IL-6_D is formed in a concentration-dependent manner when lyophilized recombinant hIL-6 is reconstituted in water. At 1 mg/mL, 5 and 10 mg/mL IL-6_D levels constitute 5−10%, 70%, and 100%, respectively, of the total hIL-6 population. Our previous results suggested that the biological activity of IL-6_D at 37 °C is due to its dissociation into active IL-6_M (*24*). As shown in an assay using human hepatoma HepG2 cells (Figure 1), stimulation of the cells for 50 min on ice with IL-6_D (5 nM) yielded no induction of tyrosine phosphorylation above the background signal from STAT3. By contrast, densitometric scanning of the bands corresponding to phosphorylated STAT3 showed 1.2-, 3.5-, and 4.2-fold increases over background for 0.8, 2, and 5 nM IL-6_M, respectively. In the presence of 5 nM IL-6_D, the increases above background for 2 and 5 nM IL-6_M were 1.4- and 2.6-fold, respectively, whereas for 0.8 nM IL-6_M no increase above background was apparent.

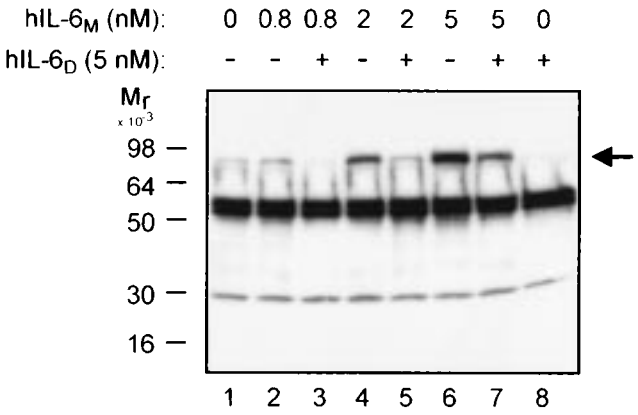

FIGURE 1: Tyrosine phosphorylation of STAT3 in response to IL-6_M and/or IL-6_D. Human hepatoma HepG2 cells were treated for 50 min on ice with various concentrations of IL-6_M in the absence or presence of 5 nM IL-6_D, as indicated. The cells were then lysed and immunoprecipitated with anti-phosphotyrosine antibodies, followed by immunoblot analysis using anti-STAT3 antibodies, as outlined under Materials and Methods. Tyrosine-phosphorylated STAT3 is indicated by the arrow.

Table 1: Sedimentation Analysis of IL-6_M and IL-6_D

	temp (°C)	MW[a] (sed eq)	MW[b] (comp)	$s_{20,w}$[a] (S) (sed velocity)	$s_{20,w}$[c] (S) (theory)	axial ratio[d]
IL-6_M	4	21400	21900	2.3	2.11	1.4
IL-6_D	4	42400	43800	3.2	3.26 (2.97)	3.5
IL-6_M	20	22500	21900	2.2	2.11	2.2
IL-6_D	20	40800	43800	3.1	3.26 (2.97)	3.6

[a] Molecular weights (MW) and sedimentation coefficients ($s_{20,w}$) were determined from sedimentation equilibrium and sedimentation velocity measurements using a value for the partial specific volume of 0.737 mL/g. Errors in $s_{20,w}$ are estimated to be ±0.1. [b] Molecular weight determined from amino acid composition. [c] Theoretical values for the sedimentation coefficients calculated using bead models (*30*) and assuming a side-by-side arrangement for the dimer. Values in parentheses refer to theoretical values for the end-to-end model. [d] The axial ratio was calculated from the experimentally determined molecular weights and sedimentation coefficients and using a value for hydration (0.41 g/g) calculated from the amino acid composition (*26*) and assuming a prolate ellipsoid.

Analytical Ultracentrifugation. Sedimentation equilibrium analysis in PBS and at 4 °C of IL-6_M and IL-6_D at starting concentrations of 0.29 and 0.54 mg/mL, respectively, yielded experimentally determined molecular weight values close to those predicted for the monomer and dimer (Table 1). These samples were subsequently equilibrated at 20 °C and reanalyzed by sedimentation equilibrium. The close agreement of the molecular weights to those estimated from the amino acid composition indicates that both the monomer and the dimer are relatively stable under these conditions. The experimentally determined molecular weight of IL-6_D at 20

°C is slightly lower than that predicted at 20 °C or experimentally determined at 4 °C (Table 1). This may represent low levels of dissociation of IL-6_D occurring over the course of the experiment (16 h).

We wanted to extend the analysis of these sedimentation studies to estimate the gross structures for IL-6_M and IL-6_D. The sedimentation coefficient of a molecule depends on the frictional coefficient, *f*, which is a function of the size and shape of the molecule (*33*). As a molecule deviates from an ideal sphere, *f* increases and the sedimentation coefficient, *s*, decreases accordingly. Theoretically, it is possible to distinguish experimentally between a long narrow rod-shaped molecule and a more globular molecule. Scans taken during the approach to equilibrium at 4 °C and at 20 °C were analyzed to obtain *s* in water at 20 °C ($s_{20,w}$) for IL-6_M and IL-6_D corrected for the effects of temperature on solution density and viscosity (Table 1). Knowledge of the molecular weight and $s_{20,w}$ values allowed estimation of the axial ratios for an equivalent prolate ellipsoid. The values obtained for IL-6_M indicate an axial ratio of approximately 2, consistent with the structure of hIL-6 revealed through X-ray crystallography (*10*) and NMR analysis (*12*). The increase in the axial ratio determined for IL-6_D (3.5 at 4 °C and 3.6 at 20 °C) suggests a more elongated structure compared to IL-6_M.

We further analyzed the sedimentation behavior of IL-6_M and IL-6_D using a method which predicts $s_{20,w}$ values (*31*) from bead models created from the PDB coordinates of proteins with known structure (*30*). For this purpose, we used a model of the murine IL-6 monomer (*28*) and simple "side-to-side" and "end-to-end" dimers based on this monomer to represent IL-6_M and IL-6_D. Although the crystal and solution structures of hIL-6 have been determined (*10, 12*), at the time of the experiment the coordinates were not available. However, predicted $s_{20,w}$ values for IL-6_M compare favorably to those obtained experimentally (Table 1), suggesting the presence of a compact structure and showing that the mIL-6 model is a good approximation of IL-6_M for these purposes. The experimental data for the dimer ($s_{20,w}$ = 3.2 S at 4 °C and 3.1 S at 20 °C) fall between those values predicted for side-by-side ($s_{20,w}$ = 3.26 S) and end-to-end ($s_{20,w}$ = 2.97 S) models. The results argue against significant unfolding in the dimer and suggest a relatively compact structure of the dimer somewhere between the two structural extremes. We compared the predicted *s* values for pairs of proteins with known structures which are closely related but which are monomeric and dimeric, respectively. These include the four-α-helical bundle proteins granulocyte macrophage colony-stimulating factor (*34*)/IL-5 (*35*) and interferon β (*36*)/IL-10 (*37, 38*), as well as the β-sheet proteins γB-crystallin (*39*)/βB2-crystallin (*40*). These data (not shown) show that predicted *s* values for dimers depend very much on the size of the dimer interface and the angle between the two halves of a dimer.

IL-6_M and IL-6_D Have Identical Levels of Secondary and Tertiary Structure. While far-UV CD spectroscopy gives information about the secondary structural content of a protein, the near-UV spectrum is a useful probe of tertiary structure, reporting on the environment of aromatic or cysteine side chains (*41*). We compared both the far- and near-UV CD spectra of IL-6_M and IL-6_D to investigate gross and fine changes in the formation of IL-6_D (Figure 2). There are no significant differences observed in either case. The

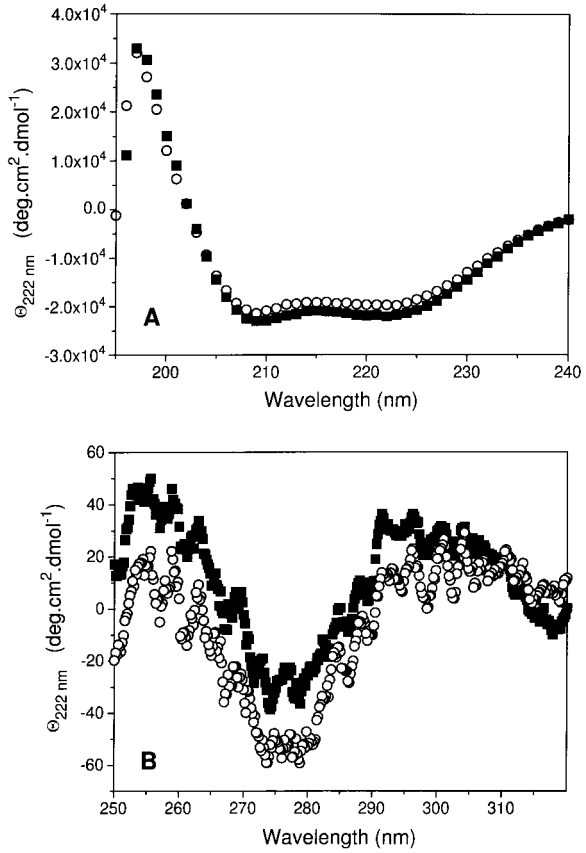

FIGURE 2: Circular dichroism analysis of IL-6_M and IL-6_D. The CD spectra of IL-6_M (○) and IL-6_D (■) were performed in PBS at 25 °C. Panel A shows the far-UV CD spectra at protein concentrations of 0.1 mg/mL using 0.1 cm pathlength cells. Panel B shows the near-UV spectra at protein concentrations of 0.5 mg/mL with 1.0 cm pathlength cells. All spectra were baseline corrected, were standardized for protein concentration, and are expressed in terms of mean residue ellipticity.

far-UV CD spectra of both proteins are essentially superimposable (Figure 2A), exhibiting the double minimum at 208 and 222 nm typical of mainly α-helical proteins, where both proteins contain 50% α-helix, 25% β-turn, and 25% random coil. Although IL-6_M has a slightly increased negative signal in the near-UV region, there are no significant features which distinguish these two spectra (Figure 2B).

The Intrinsic Fluorescence of IL-6_D Is Quenched. In contrast to the CD spectra, the tryptophan fluorescence emission spectra (excitation 295 nm) of IL-6_M and IL-6_D do show significant differences (Figure 3A). IL-6 contains only one tryptophan residue, Trp157, located at the N-terminal end of the D helix which is apparently surface-exposed (*10, 12, 42*). The intensity of the emission spectra of IL-6_D is decreased by approximately 30% from that of IL-6_M, while the wavelength maximum (λ_{max}) of IL-6_D (348 nm) is blue-shifted in comparison to that of IL-6_M (351 nm). There was no evidence of the tryptophan residues from the two separate polypeptide chains of IL-6_D being in different environments, such as the appearance of shoulders or a discernible broadening of the peak around the λ_{max} which would indicate a different maximum emission wavelength for each tryptophan, suggesting that the dimer is symmetrical.

To investigate the fluorescence phenomenon, we looked at the tryptophan quenching of IL-6_M and IL-6_D using iodide,

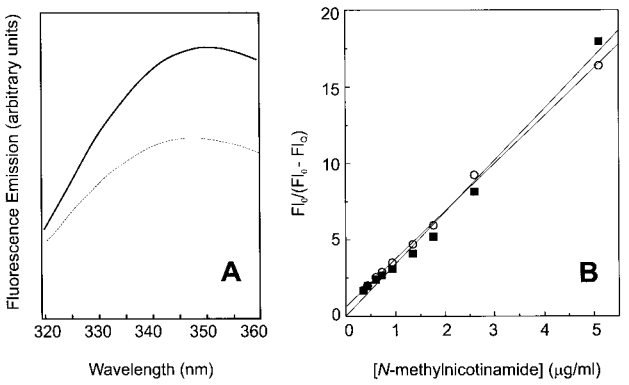

FIGURE 3: Tryptophan fluorescence of IL-6_M and IL-6_D. **(**Panel A) The fluorescence of IL-6_M (—) and IL-6_D (···) was scanned from 320 to 360 nm. (Panel B) Tryptophan fluorescence of IL-6_M (○) and IL-6_D (■) was quenched using *N*-methylnicotinamide. Data are presented as $Fl_0/(Fl_0 - Fl_Q)$ vs 1/[*N*-methylnicotinamide], where Fl_0 is the fluorescence emission intensity at 350 nm in the absence of quencher and Fl_Q is the fluorescence emission intensity at 350 nm at a given concentration of *N*-methylnicotinamide. Data are fitted to a linear equation. All data were collected at 25 °C in PBS using an excitation wavelength of 295 nm, pathlength of 5 mm, slit widths of 5 nm, and protein concentrations of 0.1 mg/mL.

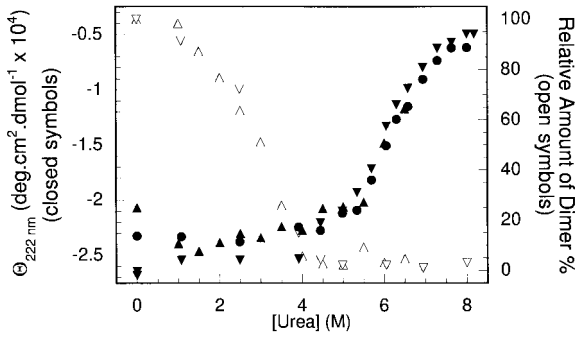

FIGURE 4: Urea denaturation of IL-6 and concomitant dissociation of IL-6_D. The equilibrium urea-induced denaturation of IL-6_M (filled circles) and IL-6_D (filled triangles) in PBS was monitored by the CD signal at 222 nm (left-hand abscissa). The same samples were subjected to size exclusion chromatography, and the relative quantities of IL-6_D remaining (open triangles) are also plotted (right-hand abscissa). Protein concentrations for experiments represented by up triangles were IL-6_D = 0.1 mg/mL and IL-6_M =0.05 mg/mL, and for down triangles were IL-6_D = 0.06 mg/mL and IL-6_M = 0.05 mg/mL.

acrylamide, and *N*-methylnicotinamide, where the latter compound can align with a fully exposed tryptophan side chain to form a charge-transfer complex (*43*). However, none of these compounds showed differential quenching of IL-6_M and IL-6_D (data for quenching by *N*-methylnicotinamide are shown in Figure 3B), suggesting that Trp157 is equally solvent-exposed in the two forms of the protein.

IL-6_D Dissociates Prior to Complete Unfolding of the Protein. We looked at the thermostability of IL-6_M and IL-6_D by equilibrium urea-induced denaturation monitored by the change of CD signal at 222 nm. Having previously observed that IL-6_D dissociates at moderate temperatures (37 °C) or in the presence of denaturant or organic solvent (*24*), we sought to also determine the extent of dissociation throughout the denaturation of IL-6_D using SEC. There are no observable differences in the urea-induced unfolding of IL-6_D and IL-6_M (Figure 4, left-hand abscissa). Both proteins exhibit a flat pretransition base line, followed by a fairly broad unfolding transition with the midpoints of unfolding ($[D]_{50\%}$) occurring at 6.0 ± 0.1 M urea. When data are fitted to conventional two-state unfolding equations (*44*−*46*), the free energies of unfolding, ΔG_{unf}, range from 5.0 to 7.4 kcal·mol^{-1}, depending on whether denaturant-dependent pre- and posttransition base lines are used. These relatively low values of ΔG_{unf} (when compared with relatively high values of $[D]_{50\%}$) stem from low values of *m*, the slope of the unfolding curve in the transition region ($m = 1.0 \pm 0.2$ kcal·mol^{-1}·M^{-1}), suggesting that unfolding is relatively uncooperative, or deviates from two-state unfolding. This is consistent with our previous observations that mIL-6 undergoes non-two-state unfolding at pH 7.4 (*46*−*48*).

The relative monomer/dimer contents of these IL-6_D samples were determined using SEC (Figure 4, right-hand abscissa). Here it can be seen that IL-6_D dissociates into its monomeric components in a sigmoidal fashion well before the major unfolding phase of the protein at 6.0 M urea, with the midpoint of dissociation at 3 M urea.

Experiments using fluorescence emission to quantitatively monitor the unfolding of IL-6_M and IL-6_D are inconclusive because only small changes occur with respect to the fluorescence emission intensity and λ_{max} (data not shown). However, in qualitative terms, λ_{max} of IL-6_D (348 nm) undergoes a red shift with increasing concentrations of urea to converge with the λ_{max} of IL-6_M (351 nm) by 4 M urea, after which the two proteins become indistinguishable, undergoing the red shift of λ_{max} typical of global unfolding (*49*) above 6 M urea, which is consistent with IL-6_D dissociating prior to the total unfolding of the protein. We do not observe the unusual fluorescence characteristics exhibited by mIL-6 under the same equilibrium unfolding conditions (*46*), which are attributable to a second tryptophan residue at position 34 in that protein (*47*). Indeed, the fluorescence-monitored unfolding of hIL-6 resembles that of a mIL-6 mutant protein in which Trp34 has been mutated to alanine (*47*).

Dissociation of IL-6_D by Increased Temperature or the Presence of Urea. Previous observations have shown that IL-6_D maintained at 4 °C is stable; at 25 °C, IL-6_D is stable for up to several hours, but at 37 °C, it dissociates into IL-6_M (Figure 5A). There were no discernible differences between the dissociation at protein concentrations of 0.48 and 0.048 mg/mL, but the resultant dissociation rates do not fit to a simple two-state dissociation model. Control data, where IL-6_D is incubated at 4 °C, show no dissociation over the same time scale. Given that urea can also cause the dissociation of IL-6_D, we examined the rates of dissociation caused by the 10-fold dilution of IL-6_D into buffer or buffer containing 3 or 5 M urea at 25 °C. In these cases, dissociation into IL-6_M occurred at a rate which approximates a double exponential decay (Figure 5B; Table 2). The rates of both phases of decay and the amplitude of the faster rate all increase with increasing urea concentration; however, the amplitude of the slower rate decreases with increasing urea concentration. The dissociation of the dimer in the absence of urea suggests that ambient temperature can affect monomer formation, but that it is greatly enhanced by the presence of denaturant. At present, we are unable to ascertain the cause of the slower rate, but suggest that the faster rates are related to the extent of unfolding in the protein. In a separate experiment, IL-6_D in PBS was diluted 5-, 10-, or 20-fold with PBS. After 1 and 5 h at 25 °C, the dimer contents of

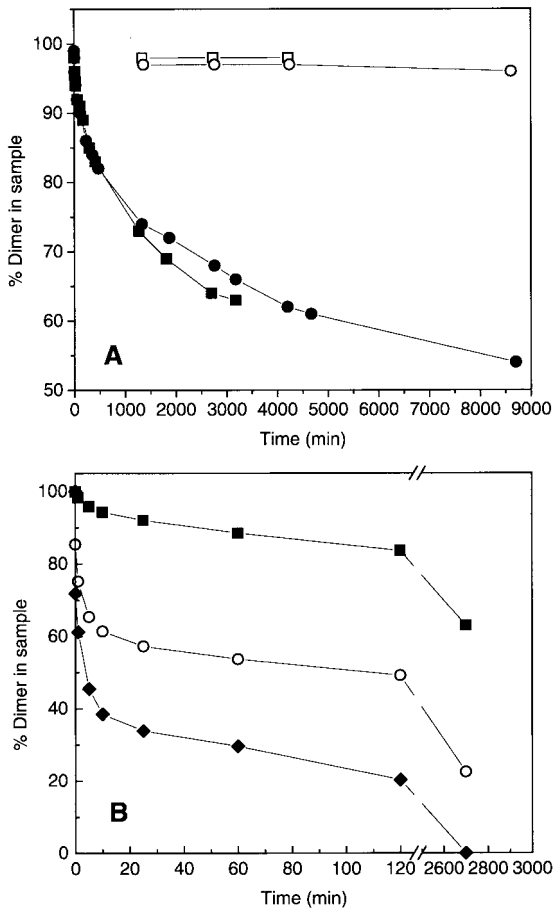

FIGURE 5: Time course for the dissociation of IL-6_D at 37 °C and by urea at 25 °C. (Panel A) IL-6_D at 0.048 mg/mL (squares) and 0.48 mg/mL (circles) was placed at 37 °C (solid symbols) and 4 °C (open symbols) and analyzed for dimer vs monomer content by SEC at the indicated time points. Data are shown as line plots and are not fitted to any equation. (Panel B) IL-6_D was diluted into PBS containing 0 M (■), 3 M (○), and 5 M (◆) urea at 25 °C. Aliquots taken at the indicated time points were analyzed for dimer content by SEC. Data are fitted to a double exponential decay.

Table 2: Rates of Dissociation of IL-6_D in PBS or PBS Containing 3 or 5 M Urea at 25 °C

[urea] (M)	A_1[a]	R_1[a] (min^{-1})	A_2[a]	R_2[a] (min^{-1})
0	14 ± 2	0.024 ± 0.009	85 ± 2	$(1.1 \pm 0.1) \times 10^{-4}$
3	28 ± 3	0.1 ± 0.05	55 ± 2	$(3.3 \pm 0.6) \times 10^{-4}$
5	32 ± 1	0.34 ± 0.04	40 ± 1	$(5.4 \pm 0.5) \times 10^{-3}$

[a] The dissociation of IL-6_D was induced by diluting IL-6_D into the indicated concentrations of urea at time zero. The relative quantities of IL-6_D and IL-6_M at each time point were estimated by SEC. Rates and amplitudes of the dissociation of IL-6_D were calculated by fitting the percentages of IL-6_D remaining to a double exponential decay: $D = A_1 \exp(-R_1 t) + A_2 \exp(-R_2 t)$, where D is the percentage of IL-6_D remaining, t is time in minutes, and A_1 is the amplitude of the faster decay, R_1, while A_2 is the amplitude of the slower decay, R_2.

all three diluted solutions were indistinguishable from that of the nondiluted control solution (data not shown).

Limited Proteolysis. Limited proteolysis was employed to further investigate possible differences between IL-6_M and IL-6_D and to try to define the dimer interface. Limiting proteolysis to restrict cleavage to accessible and flexible regions of a protein can be used as a conformational probe (*50*). This approach has been used previously to identify separate domains of large proteins, or to determine fine structural detail, such as conformational changes in folding intermediates (reviewed in ref *50*). Initially we performed limited proteolysis of the monomer and dimer at 25 °C, taking samples over a series of time points from 1 min up to 2 h, and using several broad-spectrum proteases (trypsin, pepsin, and thermolysin). With this approach, we hoped to find clearly defined differences in the accessibility of the two forms of IL-6 to proteases, which could help us to identify the dimer interface. However, the RP-HPLC profiles of partially digested IL-6_D and IL-6_M were identical (data not shown). Given that IL-6_D dissociates at low to moderate concentrations of urea, we also looked at the limited thermolytic digestion of IL-6_M and IL-6_D in increasing concentrations of urea, looking for new sites of proteolytic attack which would represent differences between the monomer and dimer as the proteins unfold. Although the partial proteolysis of IL-6_M and IL-6_D was examined over a large range of urea concentrations, we were unable to detect any such differences. We were able to identify cleavage sites from the partial proteolysis of IL-6_M and IL-6_D at low concentrations of urea, using N-terminal sequencing and/or mass spectrometry of the resultant peptides (data not shown), which were scattered over most of the surface of the protein. These data suggest that the surface area buried by the dimer interface must be small.

DISCUSSION

Antagonistic Behavior of IL-6_D. We have previously shown that IL-6_D is biologically active at 37 °C, albeit with an 8-fold lower activity than IL-6_M, and proposed that this was due to the dissociation of the inactive IL-6_D into the active IL-6_M at 37 °C (*24*). Using the same STAT3 tyrosine phosphorylation assay on ice, where there is essentially no dissociation, we now clearly show that IL-6_D exhibits negligible activity. In addition, it can prevent IL-6_M activity, and is thus shown to be an IL-6 antagonist.

The Four-α-Helical Bundle Structure of IL-6_M Is Maintained in IL-6_D. Other than the obvious increase in molecular weight and the change in axial ratios estimated from analytical ultracentrifugation studies and the different fluorescence λ_{max} values, the physical characteristics of IL-6_M and IL-6_D are essentially identical. Both proteins exhibit the behavior of compact proteins in analytical ultracentrifugation studies; they contain identical levels of secondary and tertiary structure, have identical urea denaturation profiles as monitored by far-UV CD, and show the same patterns of limited proteolysis by a number of proteases. All of these properties suggest that IL-6_D comprises two IL-6_M subunits, joined in a manner which does not perturb the basic structure of the four-α-helical bundle. The ability of IL-6_D to bind two receptor molecules (*24*) and our inability to detect different λ_{max} values for the Trp residue in each protein chain of the dimer suggest that the IL-6_D is symmetrical.

Fluorescence Properties Imply That Trp157 Is Involved in the Dimer Interface. The fluorescence λ_{max} of IL-6_M was shifted to a shorter wavelength in IL-6_D (Figure 3A). Such blue-shifts are normally associated with the transfer of the tryptophan side chain into a more hydrophobic environment and would usually, but not always, be associated with an increase in emission intensity (*49*). However, the inability to differentially quench tryptophan fluorescence in IL-6_M and

IL-6_D (Figure 3B) using several small molecule external quenchers suggests that Trp157 is not buried by the dimer interface. It is likely that the blue-shift in λ_{max} and the reduced emission intensity of IL-6_D are caused by residues which can quench tryptophan fluorescence being brought into the close proximity of Trp157 as a result of dimer formation, either from the opposite chain or as a result of local conformational changes in the same chain. While histidine and cysteine are often recognized as residues which can quench tryptophan fluorescence, proline, methionine, glutamine, asparagine, arginine, serine, threonine, glycine, lysine, valine, and alanine can all do so, albeit to lesser extents (*51, 52*). Potential quenching residues which are located at the top of the molecule (*12*) include Cys44, Asn45, Lys46, Asn48, Met49, Cys50, Gln152, Gln154, Asn155, Gln156, and Gln159. It might be expected that changing the microenvironment of a tryptophan residue as a result of dimerization should have an effect on the near-UV CD spectrum of IL-6_D. However, each IL-6 protein chain contains four Cys residues (which form two disulfide bonds), three Tyr, and seven Phe residues which can also contribute to the near-UV spectrum (*41*) and which could obscure any effects related to Trp157 in IL-6_D. Thus, Trp157 probably lies close to, but is not buried by, the dimer interface.

The ability of IL-6_D to bind the sIL-6R, but its inability to induce the formation of a hexameric IL-6/sIL-6R/sgp130 complex (*24*), provides further information for the identification of the IL-6_D interface. *Site I*, which binds the IL-6R and encompasses part of the A/B loop and the C-terminal end of helix D (reviewed in ref *3*), is clearly not affected by dimer formation. However, it is likely that *site II*, comprising residues in the A and C helices, and/or *site III*, encompassing residues from the A/B and C/D loops and the N-terminal end of helix D (reviewed in ref *3*), are probably obscured by the dimer interface, either by direct involvement in the interface or by steric effects. Notably, Trp157, which is implicated as lying close to the dimer interface by fluorescence studies, is also close to *site III*.

Nature of the IL-6_M ↔ IL-6_D Equilibrium. The dissociation of IL-6_D occurs under conditions where the protein is partially destabilized (e.g., at moderate temperatures or in the presence of moderate concentrations of denaturant), but not fully unfolded (Figure 4). That IL-6_D is formed by reconstitution from a lyophilized state suggests that dimerization of IL-6_M also occurs when the protein is partially unfolded. Oligomeric proteins have been described as generally forming by the association of preformed monomers with some intramolecular rearrangement to achieve maximum packing density and minimum hydrophobic surface area (*53*). However, there are many instances where dimers form either by a two-state mechanism, where the protein exists only as unfolded monomers or a folded dimer, or by a three-state mechanism, where monomerization/dimerization takes place when the protein is in a partially unfolded state (reviewed in ref *54*). The dimerization/dissociation of the IL-6 process probably follows a scheme such as that shown in Figure 6, where the folded (F) monomer or dimer is destabilized to form a partially unfolded intermediate (I) state (or collection of states) which contains nativelike levels of α-helix, dimeric forms of which will be favored at high protein concentrations (>2−3 mg/mL) and monomeric forms of which will be favored at low concentrations (<2 mg/mL).

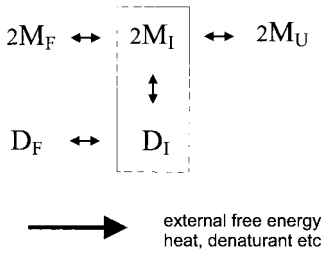

FIGURE 6: Scheme for the formation and dissociation of IL-6_D partially unfolded intermediates. M is the monomer, D is the dimer, F represents fully folded state, U represents fully unfolded state, and I represents partially unfolded or intermediate state (or states). The boxed area indicates where dimerization/dissociation takes place. The arrow indicates increased free energy of the system.

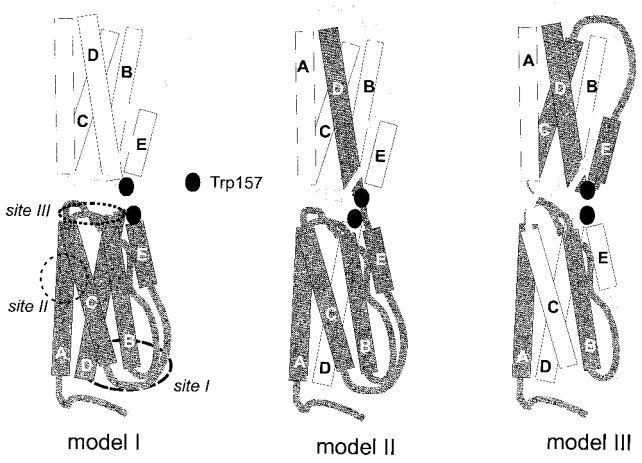

FIGURE 7: Possible dimer formation through the top of the IL-6 molecule. Models shown are sketches only, where long rectangles represent helices (labeled). Binding sites are indicated on one four-α-helical bundle unit only, but apply equally to all bundle units. Two separate polypeptide chains are represented by white/light gray and dark gray, respectively.

Dissociation occurs fairly slowly (Table 2; Figure 5), while differential scanning microcalorimetric experiments (data not shown) reveal no differences between the thermal denaturation of IL-6_M and IL-6_D, indicating that the monomer and dimer probably have similar free energies, but are separated by a reasonably high kinetic free energy barrier.

IL-6_D May Form a 3D Domain-Swapped Dimer. The fluorescence data and antagonistic behavior of IL-6_D clearly indicate that the dimer interface lies close to Trp157 at the top of the molecule (away from the N- and C-termini of the protein). Estimates of axial ratios derived from experimental *s* values suggest that IL-6_D is rodlike rather than globular. The simplest interpretation of these data is that IL-6_D is formed by the contact of two IL-6_M molecules through the top of each monomer (Figure 7, model I). Another member of the four-α-helical bundle family, CNTF is biologically active as a monomer, but forms a noncovalent dimer at protein concentrations >0.9 mg/mL (*55*). The crystal structure of dimeric CNTF shows it to be formed by the contact of two monomers arranged in a "top-to-tail" fashion, where a large dimer interface (1038 $Å^2$) is formed by the contact of residues in the B and C helices of opposite protein chains (Table 3, *55*), i.e., a compact "side-to-side" dimer. While the existence of a closely related contact dimer might appear to support a simple model for IL-6_D (Figure 7, model I), it has been experimentally shown that the topology is

Table 3: Domain-Swapped and Other Dimeric Four-α-Helical Bundle Proteins

protein[a]	disulfide bonds	site of dimer interface[b]	angle between dimer halves (deg)	swapped elements in each bundle[a]	active form
		Domain-Swapped			
IL-5	2	bottom	≈180	chain$_1$: A, B, C, and β_1 chain$_2$: D and β_2	dimer
INFγ	−	side-by-side, C	55	chain$_1$: A, B, C, and α_1 chain$_2$: α_2 and D	dimer
IL-10	−	side-by-side, C	55	chain$_1$: A, B, C, and α_1 chain$_2$: α_2 and D	dimer
		Non-Domain-Swapped			
M-CSF	1	top	180	none	dimer
CNTF	−	top-to-bottom, B and C helices	antiparallel	none	monomer[c]

[a] References for protein structures are as follows: IL-5, (*35*); INFγ, (*58*−*60*); IL-10 (*37*, *38*); M-CSF (*56*); CNTF (*55*). [b] The following terminology is used to describe the structure of the members of the four-α-helical bundle cytokine family. The four main helices, starting from the N-terminus, are referred to as A, B, C, and D. Additional helices and β-strands are referred to as α_1 and β_1, respectively, if they occur in the A−B loop and α_2 and β_2 if they occur in the C−D loop (note: helix E in IL-6 corresponds to helix α_2). The bottom of the helix is that end of the four-α-helical bundle which contains the N-terminus of the A and B helices and the C-terminus of the C and D helices, while the "top" is that end of the four-α-helical bundle which contains the C-terminus of the A and B helices and the N-terminii of the C and D helices. Chain$_1$ refers to the first polypeptide chain in each four-α-helical bundle; chain$_2$ refers to the second polypeptide chain in each four-α-helical bundle. [c] The CNTF dimer is formed at protein concentrations >0.9 mg/mL, but has a large dimer interface of 1038 Å^2 and appears to lack the metastable nature of IL-6$_D$ (*55*).

likely to be more complex. First, we were unable to detect differential susceptibility of IL-6$_D$ and IL-6$_M$ to limited proteolysis, either in buffer or in buffer containing urea, and cleavage sites identified to date are scattered over most of the surface of the molecule, suggesting that the dimer interface is small. Second, the dimer interface of IL-6 appears to involve the top of the molecule close to Trp157 rather than the side of the four-α-helical bundle. Third, IL-6$_D$ is metastable—it dissociates only under conditions where the protein is destabilized or partially unfolded (e.g., by increased temperature or the addition of denaturant), but not simply as a result of dilution. It seems unlikely that such a stable dimer could be formed through a small dimer interface. In the case of two other four-α-helical bundle cytokines which form stable dimers through an interface at the ends of the bundle, macrophage colony-stimulating factor dimer (M-CSF; *56*) is linked by interchain disulfide bonds, while IL-5 (*35*) forms interchain disulfide bonds, and additionally interchanges elements of secondary structure between bundles (Table 3) to form an extremely large dimer interface (≈7000 Å^2; *35*).

Given the above properties of IL-6$_D$ and that dissociation (and presumably formation) of IL-6$_D$ occurs when the protein is partially destabilized or partially unfolded but retains nativelike levels of secondary structure, suggests that IL-6$_D$ may be formed in a manner similar to that of IL-5. One or more helices in each bundle may be interchanged to form a large dimer interface between the two protein chains, accounting for the stability of IL-6$_D$, but a small interface between the two bundles, allowing IL-6$_D$ to maintain most of the structural characteristics of IL-6$_M$. This phenomenon, termed 3D domain-swapping, where at least one secondary structural element of a protein is replaced by the same element(s) from an identical protein chain, has been observed in a number of proteins with very different structures (reviewed in ref *57*), including several other members of the four-α-helical cytokine family (Table 3): interleukin-5 (*35*), interferon gamma (*58*−*60*), and IL-10 (*37*, *38*). It has been proposed that 3D domain-swapping is a mechanism by which monomeric proteins can evolve to become stable dimers or higher oligomers (*54*, *57*), where the length of hinge loops (stretches of the protein chain between the swapped elements) plays an important role in determining whether the monomeric or 3D domain-swapped form of the protein is stable (*57*).

The top of IL-6 contains three loop regions (between helices A and B, B and C, as well as E and D), providing an obvious means by which two monomers could maintain secondary and tertiary structural content, but could interchange helices to become a domain-swapped dimer which blocks *site III* (Figure 7, models II and III). At present, we cannot distinguish between an arrangement involving only the interchange of the C, E, and D helices through a conformational change in the B−C loop (model III), or an exchange of only the D helices through a conformational change in the short loop between the E and D helices (model II).

Role of Cytokine Dimers in Cell Signaling. While receptor dimerization is understood to be the method by which cytokines trigger cytoplasmic signaling cascades (*61*, *62*), the role of cytokine dimers is less clear. Several cytokines are active as dimers (including IL-5, M-CSF, IFNγ, IL-10). In other systems such as IL-6 (*15*, *16*), CNTF (*63*), interleukin-11 (*64*), and G-CSF (*65*, *66*), each receptor complex appears to contain two molecules of the respective monomeric cytokine, but there is no evidence of contact between these monomers.

Cytokine dimer formation could facilitate receptor dimerization in these complexes in several different ways. First, dimers could provide a means of extending the number of sites for the binding of multiple receptors, or for tailoring receptor binding. For example, IFN-γ binds two identical IFN-γ α receptors in a symmetrical fashion, leaving sufficient room for the binding of the β receptors (*60*). In the case of IL-5, the IL-5 dimer binds a single α receptor (IL-5Rα), and the binding site appears to lie primarily in one four-α-helical bundle, but also partially across the dimer interface, apparently guiding the binding of the IL-5 β receptor to that same bundle (*67*). A genetically engineered monomeric form of IL-5 has 10-fold less biological activity than dimeric IL-5, possibly due to decreased surface area for the binding of IL-5Rα (*68*). Second, monomeric cytokines may form

contact dimers in the signaling complexes, providing additional stabilizing interactions. For example, a fourth binding site has been proposed in IL-6 which would allow two IL-6 monomers to make contact (*10*). Two models of the hexameric IL-6/IL-6R/gp130 signaling complex allow this contact to take place (*16, 23*), although at present no experimental evidence has shown that this is the case. Finally, dimers of normally monomeric cytokines may serve as storage units (*55, 69*) or as a means of recruiting receptor chains prior to the formation of signaling complexes (*55*). Such dimers could form by domain-swapping in a manner similar to that proposed for IL-6.

We suggest that IL-6_D is formed by 3D domain-swapping of one or more helices through the loop regions at the top of the molecule close to, but not burying, Trp157, where the interface between the two four-α-helical bundle units is small and the angle between the axes of the two bundles is at present undetermined. Such an arrangement would explain both the stability of the dimer in the absence of a large interface and the structural similarities between IL-6_M and IL-6_D. It would also leave *site I* free for interaction with IL-6R but would prevent the binding of at least one and possibly both of the gp130 molecules to *sites II* and *III*, by either direct occlusion or steric hindrance of these sites, accounting for the antagonistic activity of IL-6_D.

ACKNOWLEDGMENT

We thank H. Treutlein for help with molecular modeling, J. S. Eddes, R. L. Moritz, and G. E. Reid for the preparation of recombinant IL-6, and A. W. Burgess for critical comment of the manuscript.

REFERENCES

1. Akira, S., Taga, T., and Kishimoto, T. (1993) *Adv. Immunol. 54*, 1−78.
2. Narazaki, M., and Kishimoto, T. (1994) in *Guidebook to cytokines and their receptors* (Nicola, N. A., Ed.) pp 56−58, Oxford University Press, Oxford, U.K.
3. Simpson, R. J., Hammacher, A., Smith, D. K., Matthews, J. M., and Ward, L. D. (1997) *Protein Sci. 6*, 929−955.
4. Hirano, T. (1994) in *The Cytokine Handbook* (Thompson, A., Ed.) 2nd ed., pp 145−167, Academic Press, San Diego.
5. Klein, B., Zhang, X.-G., Lu, Z.-Y., and Bataille, R. (1995) *Blood 85*, 863−872.
6. Moore, P. S., Boshoff, C., Weiss, R. A., and Chang, Y. (1996) *Science 274*, 1739−1744.
7. Rettig, M. B., Ma, H. J., Vesico, R. A., Põld, M., Schiller, G., Belson, D., Savage, A., Nishikubo, C., Wu, C., Fraser, J., Said, J. W., and Berenson, J. R. (1997) *Science 276*, 1851−1854.
8. Bazan, J. F. (1990) *Immunol. Today 11*, 350−354.
9. Nishimura, C., Watanabe, A., Gouda, H., Shimada, I., and Arata, Y. (1996) *Biochemistry 35*, 273−281.
10. Somers, W., Stahl, M., and Seehra, J. S. (1997) *EMBO J. 16*, 989−997.
11. Xu, G.-Y., Hong, J., McDonagh, T., Stahl, M., Kay, L. E., Seehra, J., and Cumming, D. A. (1996) *J. Biomol. NMR 8*, 123−135.
12. Xu, G. Y., Yu, H. A., Hong, J., Stahl, M., McDonagh, T., Kay, L. E., and Cumming, D. A. (1997) *J. Mol. Biol. 268*, 468−481.
13. Hibi, M., Murakami, M., Saito, M., Hirano, T., Taga, T., and Kishimoto, T. (1990) *Cell 63*, 1149−1157.
14. Bravo, J., Staunton, D., Heath, J. K., and Jones, E. J. (1998) *EMBO J. 17*, 1665−1674.
15. Ward, L. D., Howlett, G. J., Discolo, G., Yasukawa, K., Hammacher, A., Moritz, R. L., and Simpson, R. J. (1994) *J. Biol. Chem. 269*, 23286−23289.
16. Paonessa, G., Graziani, R., de Serio, A., Savino, R., Ciapponi, L., Lahm, A., Salvati, A. L., Toniatti, C., and Ciliberto, G. (1995) *EMBO J. 14*, 1942−1951.
17. Grötzinger, J., Kurapkat, G., Wollmer, A., Kalai, M., and Rose-John, S. (1997) *Proteins: Struct., Funct., Genet. 27*, 96−109.
18. May, L. T., Santhanam, U., and Seghal, P. B. (1991) *J. Biol. Chem. 266*, 9950−9955.
19. Wijdenes, J., Clement, C., Klein, B., Morel-Fourrier, B., Vita, N., Ferrara, P., and Peters, A. (1991) *Mol. Immunol. 28*, 1183−1192.
20. Rose-John, S., Schooltink, H., Lenz, D., Hipp, E., Dufhues, G., Schmitz, H., Schiel, X., Hirano, T., Kishimoto, T., and Heinrich, P. C. (1990) *Eur. J. Biochem. 190*, 79−83.
21. Rose-John, S., Hipp, E., Lenz, D., Legres, L. G., Korr, H., Hirano, T., Kishimoto, T., and Heinrich, P. C. (1991) *J. Biol. Chem. 266*, 3841−3846.
22. D′Alessandro, F., Colamonici, O. R., and Nordon, R. P. (1993) *J. Biol. Chem. 268*, 2149−2153.
23. Menziani, M. C., Fanelli, F., and De Benedetti, P. G. (1997) *Proteins: Struct., Funct., Genet. 29*, 528−544.
24. Ward, L. D., Hammacher, A., Howlett, G. J., Matthews, J. M., Fabri, L., Moritz, R. L., Nice, E. C., Weinstock, J., and Simpson, R. J. (1996) *J. Biol. Chem. 271*, 20138−20144.
25. Zhong, Z., Wen, Z., and Darnell, J. E. (1994) *Science 264*, 95−98.
26. Laue, T. M., Shah, B. D., Ridgeway, T. M., and Pelletier, S. L. (1992) in *Analytical Ultracentrifugation in Biochemistry and Polymer Science* (Harding, S. E., Rowe, A. J., and Horton, J. C., Eds.) pp 90−125, The Royal Society of Chemistry, Cambridge, U.K.
27. Schuck, P., MacPhee, C. E., and Howlett, G. J. (1998) *Biophys. J. 78* (in press).
28. Hammacher, A., Ward, L. D., Weinstock, J., Treutlein, H., Yasukawa, K., and Simpson, R. J. (1994) *Protein Sci. 3*, 2280−2293.
29. Hill, C. P., Osslund, T. D., and Eisenberg, D. (1993) *Proc. Natl. Acad. Sci. U.S.A. 90*, 5167−5171.
30. Byron, O. (1997) *Biophys. J. 72*, 408−415.
31. Garcia de la Torre, J., Navarro, S., Lopez Martinez, M. C., Diaz, F. G., and Lopez Cascales, J. J. (1994) *Biophys. J. 67*, 530−531.
32. Yang, J. T., Wu, C.-S. C., and Martinez, H. M. (1986) *Methods Enzymol. 130*, 208−296.
33. Ralston, G. (1993) *Introduction to Analytical Ultracetrifugation*, Beckman Instruments, Inc., Fullerton, CA.
34. Diederichs, K., Boone, T., and Karplus, P. A. (1991) *Science 254*, 1779−1782.
35. Milburn, M. V., Hassell, A. M., Lambert, M. H., Jordan, S. R., Proudfoot, A. E. I., Graber, P., and Wells, T. N. C. (1993) *Nature 363*, 172−176.
36. Senda, T., Shimazu, T., Matsuda, S., Kawano, G., Shimizu, H., Nakamura, K. T., and Mitsui, Y. (1992) *EMBO J. 11*, 3193−3201.
37. Zdanov, A., Schalk-Hihi, C., Gustchina, A., Tsang, M., Weatherbee, J., and Wlodawer, A. (1995) *Structure 3*, 591−601.
38. Zdanov, A., Schalk-Hihi, C., Menon, S., Moore, K. W., and Wlodawer, A. (1997) *J. Mol. Biol. 268*, 460−467.
39. Summers, L., Wistow, G., Narebor, M., Moss, D., Lindeley, P., Slingsby, C., Blundell, T., Bartunik, H., and Bartels, K. (1984) in *Peptide and protein reviews* (Hearn, M. T. W., Ed.) Vol. 3, pp 147−168, Marcell Decker, New York.
40. Lapatto, R., Nalini, V., Bax, B., Driessen, H., Lindley, P. F., Blundell, T. L., and Slingsby, C. (1991) *J. Mol. Biol. 222*, 1067−1083.
41. Kahn, P. C. (1979) *Methods Enzymol. 61*, 339−378.
42. Nishimura, C., Hanzawa, H., Itoh, S., Yasukawa, K., Shimada, I., Kishimoto, T., and Arata, Y. (1990) *Biochim. Biophys. Acta. 1041*, 243−249.
43. Deranleau, D. A., Bradshaw, R. A., and Schwyzer, R. (1969) *Proc. Natl. Acad. Sci. U.S.A. 63*, 885−889.
44. Santoro, M. M., and Bolen, D. W. (1988) *Biochemistry 27*, 8063−8068.

45. Clarke, J., and Fersht, A. R. (1993) *Biochemistry 32*, 4322−4329.
46. Ward, L. D., Matthews, J. M., Zhang, J. G., and Simpson, R. J. (1995) *Biochemistry 34*, 11652−11659.
47. Matthews, J. M., Ward, L. D., Hammacher, A., Norton, R. S., and Simpson, R. J. (1997) *Biochemistry 36*, 6187−6196.
48. Zhang, J.-G., Matthews, J. M., Ward, L. D., and Simpson, R. J. (1997) *Biochemistry 36*, 2380−2389.
49. Lakowicz, J. R. (1990) *Principles of Fluorescence Spectroscopy*, Plenum Press, New York.
50. Fontana, A., Polverino de Laureto, P., de Filippis, V., Scaramella, E., and Zambonin, M. (1997) *Folding Des. 2*, R17−26.
51. Steiner, R. F., and Kirby, E. P. (1969) *J. Phys. Chem. 73*, 4130−4135.
52. Van Gilst, M., Tang, C., Roth, A., and Hudson, B. (1994) *J. Fluoresc. 4*, 203−207.
53. Jaenicke, R. (1995) *Philos. Trans. R. Soc. London B 348*, 97−105.
54. Xu, D., Tsai, C.-J., and Nussinov, R. (1998) *Protein Sci. 7*, 533−544.
55. McDonald, N. Q., Panayotatos, N., and Hendrickson, W. A. (1995) *EMBO J. 14*, 2689−2699.
56. Pandit, J., Bohm, A., Jancarik, J., Halenbeck, R., Koths, K., and Kim, S.-H. (1992) *Science 258*, 1358−1362.
57. Bennett, M. J., Schlunegger, M. P., and Eisenberg, D. (1995) *Protein Sci. 4*, 2455−2468.
58. Ealick, S. E., Cook, W. J., Vhay-Kumar, S., Carson, M., Nagablushan, T. L., Trotta, P., and Bugg, C. E. (1991) *Science 252*, 698−702.
59. Samudzi, L. T., Burton, L. E., and Rubin, J. R. (1991) *J. Biol. Chem. 266*, 21791−21797.
60. Walter, M. R., Windsor, W. T., Nagabhushan, T. L., Lundell, D. J., Lunn, C. A., Zauodny, P. J., and Narula, S. K. (1995) *Nature 376*, 230−235.
61. Heldin, C. H. (1995) *Cell 80*, 213−223.
62. Wells, J. A., and de Vos, A. M. (1996) *Annu. Rev. Biochem. 165*, 609−634.
63. de Serio, A., Graziani, R., Laufer, R., Ciliberto, G., and Paonessa, G. (1995) *J. Mol. Biol. 254*, 795−800.
64. Nedderman, P., Graziani, R., Ciliberto, G., and Paonessa, G. (1996) *J. Biol. Chem. 271*, 30986−30991.
65. Horan, T., Wen, J., Narhi, L., Parker, V., Garcia, A., Arawaka, T., & Philo, J. (1996) *Biochemistry 35*, 4886−4896.
66. Horan, T. P., Martin, F., Simonet, L., Arawaka, T., and Philo, J. (1997) *J. Biochem. Tokyo 121*, 370−375.
67. Li, J., Cook, R., and Chaiken, I. (1996) *J. Biol. Chem. 271*, 31729−31734.
68. Dickason, R. R., and Huston, D. P. (1996) *Nature 379*, 652−655.
69. Cunningham, B. C., Mulkerrin, M. G., and Wells, J. A. (1991) *Science 253*, 545−548.

BI980127P